UFSM

REGET/UFSM
Revista Eletrônica em Gestão, Educação e Tecnologia Ambiental

V. 26 2022

ISSN 2236-1170
Acesso aberto

REGET, v. 26, e2, 2022 • https://doi.org/10.5902/2236117065265
Submitted: 14/04/2021 • Accepted: 13/09/2022 • Published: 23/12/2022

Environmental Technology

Biosorption textile wastewater employing lemon peel derivatives: data analysis and kinetic modeling

Biossorção de efluentes têxteis empregando derivados de casca de limão: análise de dados e modelagem cinética

Naiana Santos da Cruz Santana Neves[I], Ramon Vinícius Santos de Aquino[I], Ingrid Larissa Silva Santana[I], Welenilton José do Nascimento Júnior[I], Ada Azevedo Barbosa[I], Rafaela Ferreira Carvalho[I], Josivan Pedro Silva[I], Mohand Benachour[I], Otidene Rossiter Sá da Rocha[I]

[I] Universidade Federal de Pernambuco, Recife, Pernambuco, Brazil

ABSTRACT

The present work aimed to evaluate the efficiency of an agro-industrial waste biosorbent in the removal of real textile wastewater. A model sample with methylene blue and remazol golden yellow at equimolar proportions was prepared to be treated with in natura, carbonized, and activated lemon peel beads. Activated biosorbent demonstrated superior capacity and removal rates. Characterization analyses investigated the morphology and physico-chemical properties of the biomaterial. The pH (2.0) and dosage (1.6 $g.L^{-1}$) studies were carried out to select parameters for further studies. In kinetic assays, methylene blue equilibrium was reached faster than remazol golden yellow RNL. The analyses of fitting parameters indicated Elovich kinetic model to describe biosorption of the yellow dye while pseudo-first-order fit best to the blue dye biosorption data. The intraparticle diffusion model indicated that more than one step may limit biosorption kinetics. In the treatment of real textile wastewater, 94.22% of dyes removal was attained after 360 minutes of operation at the selected operational conditions. Kinetics of adsorption of real wastewater presented considerable fitting to the models with R^2 greater than 0.93. An artificial neural network model was developed to describe the removal of dyes in real wastewater with satisfactory fitting (R^2 = 0.990).

Keywords: Agro-industrial waste; Binary biosorption; Lemon peel; Neural network; Textilesynthetic dyes; Wastewater treatment

RESUMO

O presente trabalho teve como objetivo avaliar a eficiência de um biossorvente de resíduos agroindustriais na remoção de águas residuais têxteis reais. Uma amostra modelo com azul metileno e amarelo dourado remazol amarelo ouro em proporções equimolares foi preparada para ser tratada com casca de limão in natura, carbonizadas e ativadas. O biossorvente ativado demonstrou taxas de capacidade e remoção superiores. Análises de caracterização investigaram as propriedades da morfologia e da física-química do bioma material. Foram realizados os estudos de pH (2.0) e dosagem (1,6 $g.L^{-1}$) para selecionar parâmetros para estudos posteriores. Em ensaios cinéticos, o equilíbrio azul de metileno foi alcançado mais rápido que o RNL amarelo dourado remazol. As análises dos parâmetros de montagem indicaram modelo cinético elovich para descrever a biosorção do corante amarelo, enquanto pseudo-primeira ordem se encaixa melhor aos dados de biosorção de corante azul. O modelo de difusão intrapartícula indicou que mais de uma etapa pode limitar a cinética da biosorção. No tratamento de águas residuais têxteis reais, 94,22% da remoção de corantes foi atingida após 360 minutos de operação nas condições operacionais selecionadas. Cinética de adsorção de águas residuais reais apresentou considerável adequação aos modelos com R^2 superior a 0,93. Um modelo de rede neural artificial foi desenvolvido para descrever a remoção de corantes em águas residuais reais com encaixe satisfatório (R^2 = 0,990).

Palavras-chave: Biossorção binária; Casca de limão; Corantes têxteis; Rede neural; Resíduos agroindustriais; Tratamento de águas residuais

1 INTRODUCTION

In the last few decades, environmental issues have been intensified due to the increase in population and industrial activity. As a consequence, larger amounts of pollutants are discharged from industries in natural water bodies. These pollutants, such as synthetic dyes, are toxic and may harm ecosystems and threaten human health (SANDOVAL *et al.*, 2017) . Among the chemical industries, the textile sector is one of the largest consumers of dyes, and therefore, its wastewater is pointed out for some authors as the most hazardous one among the chemical industries (BARBOSA *et al.*, 2017). The main issue is the incomplete binding of the dye molecules to the tissue fibers in the coloring steps (DEHGHANI *et al.*, 2016). As a consequence, its discharge in natural waters without the required treatments represents harmful consequences to life due to their carcinogenic, mutagenic, allergenic, and toxic properties (AICHOUR *et al.*, 2018).

In addition to human health threats, they may partially color the water according to their concentration, which decreases solar light penetration and subsequently hinders photosynthesis and disturbs aquatic life (HISAINDEE *et al.*, 2013). They also enhance water organic content and inhibit oxygen to dissolve in the medium (HOLKAR *et al.,* 2016). Most

of them also exhibit high stability to conventional water treatment methods due to their complex structure. Thus, alternative ways that allow effective removal of these chemicals are being investigated (AHMAD *et al.,* 2018).

Adsorption has been pointed out as a feasible technique in wastewater treatment. The main advantages associated with the operation are the simple operation methods and the wide range of low-cost, highly abundant, and renewable materials to be applied as adsorbents (GISI *et al.,* 2016; ANDRADE *et al.,* 2020). Activated carbon presents superior adsorption capacity and therefore, it is the most employed adsorbent in large operation processes, although, the resource is limited since the material does not come from renewable sources (AMIN; MATER, 2009).

Agro-industrial waste, marc, bran, and fruit peels have been investigated in the preparation of adsorbent particles as an alternative to commercial activated carbon (WANG *et al.,* 2018). Literature has reported several types of biomass from lemon peels (BHATNAGAR *et al.,* 2009), grape (SAEED *et al.,* 2010), Limetta (SUDAMALLA; PICHIAH; MANICKAM, 2012), pineapple (LUTPI *et al.,* 2013), breadfruit (CHIENG; LIM; PRIYANTHA, 2015), cucumber (BELLO; AHMAD; SEMIRE, 2015), banana (SAHIBZADA *et al.,* 2016), fruit peel of plant hydnocarpus pentandra (NAYAK *et al.,* 2020) and pomegranate (GHIBATE; SENHAJI; TAOUIL, 2021) with considerable potential to remove pollutants from aqueous media. These materials are, in general, readily available, recyclable, sustainable, and environmental-friendly (LI *et al.,* 2018).

Real wastewater adsorption is still scarce in the literature. Many studies apply synthetic samples (most of them are single systems containing only one dye species) which may not correspond to the behavior of real water matrices (SHARMA *et al.,* 2018). Synthetic dye adsorption is able to provide optimization for operational parameters of the process, such as samples containing Methylene Blue (MB) and Remazol Gold Yellow (RYG), which are already explored in the literature by a variety of adsorbents in single-adsorbate systems (LOW; TAN, 2018). This work aimed to develop biosorbents from lemon peels and evaluate their efficiency in the treatment of a real

wastewater sample from the textile industry. MB and RYG binary systems were studied in order to select the parameters of the operation. In addition, kinetic modeling and an Artificial Neural Network (ANN) model were investigated for the treatment data.

2 EXPERIMENTAL

MB and RYG were acquired from Casa da Química Indústria e Comércio LTDA (Brazil) DYSTAR (Brazil), respectively, to prepare model samples. The real wastewater was collected from a jeans dying factory in Toritama (Pernambuco, Brazil) and stored at 5°C in the absence of radiation.

The removal rates of dyes were evaluated by UV-Visible spectroscopy (Spectroquant Pharo 300). RYG and MB were identified at 410 e 663 nm, respectively. Aromatic content was also estimated at the wavelength of 254 nm. The samples were centrifuged (Novatecnica NT812) before the analytical procedure. The adsorption capacity q for each dye was calculated according to Equation 1.

$$q_i = \frac{[C_{i,0} - C_i(t)]V}{m} \quad (1)$$

Where $C_i(t)$ is the concentration of dye i at time t ($mg.L^{-1}$), $C_{i,0}$ is the initial concentration of dye i ($mg.L^{-1}$), V is the total volume of metal sample (L) and m is the biosorbent mass (g).

2.1 Biosorbent preparation

Three biosorbents were investigated: *in natura* (N), activated (A), and carbonized (C) lemon peel derivatives. Initially, the peel was washed with distilled water and dried at 100 ± 1°C in a forced air circulation furnace (Marconi MA035/1). The material was then powdered in a knife mill (Tecnal) as described by Nascimento *et al.* (2014). The particles were sieved in Tyler meshes (26 and 32) to provide particles with a diameter

range from 0.5 to 1.0 mm and then washed and dried in the furnace at 100°C for 2 hours to prepare biosorbent N.

To prepare biosorbent A, particles of biosorbent N were added to an orthophosphoric acid sample (85%) (H_3PO_4 acquired from Merck) at the proportion of 1:1 (w/v) and activated in a muffle furnace at 250°C for 90 minutes (BRITO *et al.,* 2018). The activated samples were washed with HCl (37%) acquired from Química Moderna and later dried in the furnace at 105°C for 120 minutes. To prepare biosorbent C, particles of biosorbent N were calcined in a muffle furnace at 250°C for 90 minutes.

2.2 Biosorbent characterization

The biosorbents N, A, and C were characterized to collect information about its surface morphology by Scanning Electron Microscopy (SEM). Modification in functional groups according to the three different preparations were analyzed by Fourier-Transform Infrared Spectroscopy (FTIR) in a Brucker Tensor 27 coupled with attenuated total reflectance. The spectra were generated with 32 scannings per sample in the range of 500-4000 cm^{-1}.

Thermogravimetric analyses were carried out to investigate the materials' mass loss profile according to the temperature. Around 10 mg of each biosorbent particles were evaluated in the range of 25 up to 900°C in a Perkin Elmer STA 6000 simultaneous thermal analyzer. The Specific Surface Area (SSA) was determined by the Brunauer, Emmett, and Teller (BET) method. The volume and average pore size of biosorbent were determined in a Quanta Chrome NOVA surface area analyzer by nitrogen physisorption/desorption isotherms at 77 K.

To investigate the ionic profile of the biosorbent with pH dependence, 0.1 g of each biosorbent was brought into contact with 25 mL of samples (pH ranged from 2 to 10). The samples were prepared with HCl (0.1 $mol.L^{-1}$) and NaOH (0.1 $mol.L^{-1}$). The systems were stirred at 200 rpm for 24 hours to determine pH_{PZC} (NASCIMENTO *et al.,* 2014). The pH of the samples was evaluated at the beginning and the end of the assays.

2.3 Selection of operational parameters

The influence of pH and dosage was investigated in the biosorption capacity. The model sample was prepared with 10 mg.L^{-1} of each dye (MB and RYG) and 50 mL of samples were treated with 0.2 g of biosorbent for 2 hours at 200 rpm and 25°C. Samples were adjusted to pH = 2, 4, 6, 8, and 10 (NASCIMENTO *et al.*, 2014).

The pH in which the highest q_{MB} and q_{RYG} values were achieved was selected to perform the dosage study. The biosorbent mass was ranged from 1.2 to 20 g.L^{-1} for the 5 model sample of synthetic dyes at 10 mg.L^{-1} each. This study was performed with biosorbents N and A.

To evaluate the kinetics of adsorption, 240 mL of the model sample at concentrations of 5, 10, and 15 mg.L^{-1} of each dye were treated for 360 minutes at room temperature (25°C) and 200 rpm.

2.4 Kinetic modeling of model sample

To investigate the biosorption temporal dependence and the rate-limiting steps of the operation, the pseudo-first-order (PFO), pseudo-second-order (PSO), intraparticle diffusion, and Elovich kinetic models were fit to the data. PFO fitting, described by Lagergren (1898), is based on the proportionality of free active sites and adsorption capacity (Equation 2) (SHARMA *et al.*, 2019).

$$\phi(x) = \frac{2}{1+e^{-x}} - 1 \quad \frac{dq_t}{dt} = k_1(q_e - q_t) \tag{2}$$

Where k_1 is the adsorption rate constant (min^{-1}), q_e is the biosorption capacity at the equilibrium state (mg.L^{-1}) and q_t is the biosorption capacity at time t (mg.L^{-1}).

The PSO model takes into consideration the occurrence of chemical interactions as responsible for the efficiency and the rate dependence of the physico-chemical interactions between adsorbate and the active sites (Equation 3).

$$\frac{dq_t}{dt} = k_2(q_e - q_t)^2 \tag{3}$$

Where k_2 is the second-order adsorption rate constant (g.mg^{-1}.min^{-1}).

Elovich model (Equation 4) is commonly applied for systems that exhibit heterogeneous adsorption sites. It is based on the decrease in the rate of adsorption along time due to the filling of active sites on the surface (SHAKOOR; NASA; TAIWAN, 2016).

$$\frac{dq_t}{dt} = \alpha e^{(-\beta q_t)} \tag{4}$$

Where α is the initial rate adsorption ($mg.g^{-1}.min^{-1}$) and β is the desorption rate constant ($g.mg^{-1}$).

When intraparticle diffusion is the rate-limiting step of adsorption, the removal rates of adsorbate is proportional to the time square root. Thus, biosorption capacity relation with intraparticle diffusion rate constant is described by Equation 5 according to Weber and Morris (WEBER; MORRIS; 1963).

$$q_t = k_{dif} t^{0.5} + C \tag{5}$$

Where k_{dif} is the intraparticle diffusion rate constant ($mg\ g^{-1}\ min^{-1/2}$) and C ($mg.g^{-1}$) is a constant related to the resistance to diffusion.

To evaluate the model fitting, the Correlation Coefficient (R^2) and corrected Akaike Information Criteria (AICc) were estimated for each kinetic profile (Equations 6 and 7, respectively). AICc represents the degree of losses of the model concerning the experimental data in a group of models, thus, the lowest AICc values may indicate the most suitable model among the tested ones (BONATE, 2011).

$$R^2 = 1 - \frac{\sum_{i=1}^{N} (q_{\exp} - q_{calc})^2}{\sum_{i=1}^{N} (q_{\exp} - q_A)^2} \tag{6}$$

$$AIC_c = N \ln \frac{\sum_{i=1}^{N} (q_{\exp} - q_{calc})^2}{N} + 2p + \frac{2p(p+1)}{N - p - 1} \tag{7}$$

Where q_{exp} is the experimental biosorption capacity ($mg.g^{-1}$), q_{calc} is the calculatedbiosorption capacity according to the model ($mg.g^{-1}$), q_A is the global average biosorption capacity of the data ($mg.g^{-1}$), N is the amount of the sample and p is the number of parameters in the model.

2.5 Textile wastewater biosorption

From the previous assays with the model sample, the adsorption operation with real wastewater was investigated. The wastewater sample was evaluated before the assays by UV/Visible spectroscopy and 200 mL of samples were treated in the selected experimental conditions of pH and biosorbent dosage. Samples were collected at 0, 15, 30, 45, 60, 90, 120, 150, 180, 240, 300, and 360 minutes. Modeling of the adsorption data was made with PFO, PSO, Elovich, and intraparticle diffusion models and the results were compared to the model sample modeling.

For the development of an ANN model, a software named Neural Educator, developed by the research group and employed in previous works with Advanced Oxidation Processes (BARBOSA *et al.,* 2017; AQUINO *et al.,* 2019) was for the first time employed in an adsorption process. Two feedforward ANN-type were assessed, (1:3:2) and (1:2:2). The first number means the input, which in this work was the time, and the last number is the output values, which were set to be the removal rates of dyes and aromatic content. The middle number represents the number of neurons (hidden layers), which ranged from 2 to 3. The activation sigmoidal function can be seen in Equation 8.

$$\phi(x) = \frac{2}{1+e^{-x}} - 1 \qquad (8)$$

The learning method of the network consisted of a set of random and genetic algorithm methods [29] that allows a greater fit to the parameters, although it requires higher computational efforts. To evaluate the fitting, the correlation coefficient (R^2) was taken into consideration. The training values were normalized to the range [-1, 1] for both input and output sets of data (BISHOP, 1996).

3 RESULTS AND DISCUSSION

3.1 Biosorbent characterization

The SEM images and the FTIR spectrum of three lemon peel-based biosorbents and the adsorption/desorption isotherms of N_2 for the biosorbent A are exhibited in Fig. 1.

Figure 1 – Scanning electron microscopes of the lemon peel *in natura* (a), carbonized (b), and activated (c) magnified 1500 times. (d) FTIR spectra of the three lemon peel-derived biosorbents; (e) N_2-physisorption/desorption isotherms for activated lemon peel biosorbent

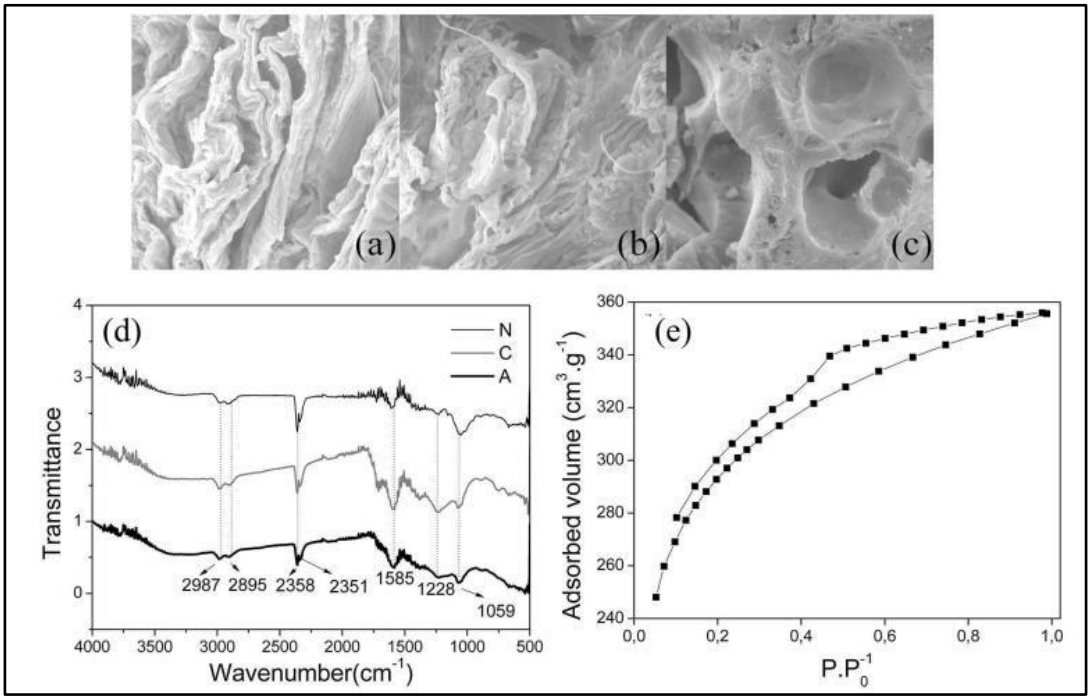

Source: Authors (2021)

Comparing Fig. 1a and b, it is possible to conclude that the thermal treatment (carbonization) promoted a reduction in lamellar structures. The activation process (Fig. 1c) employing phosphoric acid promoted irregular pore formation when compared to *in natura* biosorbent. Similar results were reported by Deng *et al.* (2010) in the activation of cotton stalks with the same activation agent. Biosorbent A demonstrated the most

suitable surface structure to the treatment of dyes in aqueous matrices since the surface area is enhanced by the carbonization process. The formation of pores is promoted by the evaporation of the chemicals.

Modifications in functional groups of the surfaces can be observed in the FTIR spectra (Figure 1d) by the increase/reduction in the intensity of the vibrational frequency of the characteristic bands. The bands ranging from 3000 to 2900 cm^{-1} are characteristic from the stretching of the hydrogen-carbon bond in $–CH_3$ and $-CH_2$ groups in biomass (SOLOMONS; FRYHLE, 2012). The symmetrical axial deformation of CO_2 bound in the aryl group of lignin is observed between 2400-2300 cm^{-1} (PEREIRA *et al.*, 2017).

Regarding the band at 1585 cm^{-1}, the stretching of carbon-carbon double bond did not present significant differences in biosorbent N and A. The asymmetrical stretch =C=O-C in lignin (at 1228 cm^{-1}) demonstrated a broader band for C and less intense for biosorbent A when compared to the N band (ZHANG *et al.*, 2017). The use of dehydration agents at high temperatures may have favored the degradation of these groups on the surface of the biosorbent. A reduction can be noticed at 1059 cm^{-1} for the biosorbents C and A, which corresponds to the oxygenated groups –C-O and C=O. These results may be due to the severe thermal treatment used in the materials (SOLOMONS; FRYHLE, 2012).

The isotherms for biosorbent N and C were not possible to be obtained. The predominance of lamellar structures in the biosorbent N and the absence of cavities in C (according to Fig. 1a and b) corroborates with these results. Fig. 1e exhibits the isotherm for the activated lemon peel in accordance with the surface porosity detected in the micrographs (Fig. 1c). The isotherms exhibited similar characteristics of type IV according to IUPAC classification (THOMMES *et al.,* 2015). The results indicate the presence of hysteresis phenomena in capillary condensation. This is common when the material is in the transition of microporosity and mesoporosity, which allows the adsorption of compounds in a range of 20-500 Å of molecular size.

The biosorbent A is classified as a mesoporous material according to IUPAC since it presented surface area, pore volume distribution, and average pore diameter of 931.8 m^2g^{-1}, 0.55 $cm^3.g^{-1}$ e 23.62 Å, respectively (THOMMES *et al.*, 2015). Goswami and Phukan (2017) have also reported elevated surface area biosorbent from the activation process of tea leaves with H_3PO_4.

Thermogravimetric analyses allowed the evaluation of the decomposition of the material at temperatures up to 900°C (Fig. 2).

Figure 2 – Mass loss profiles (TG) and Derivative Thermogravimetry (DTG) for lemon peel particles (a) *in natura*, (b) carbonized, and (c) activated

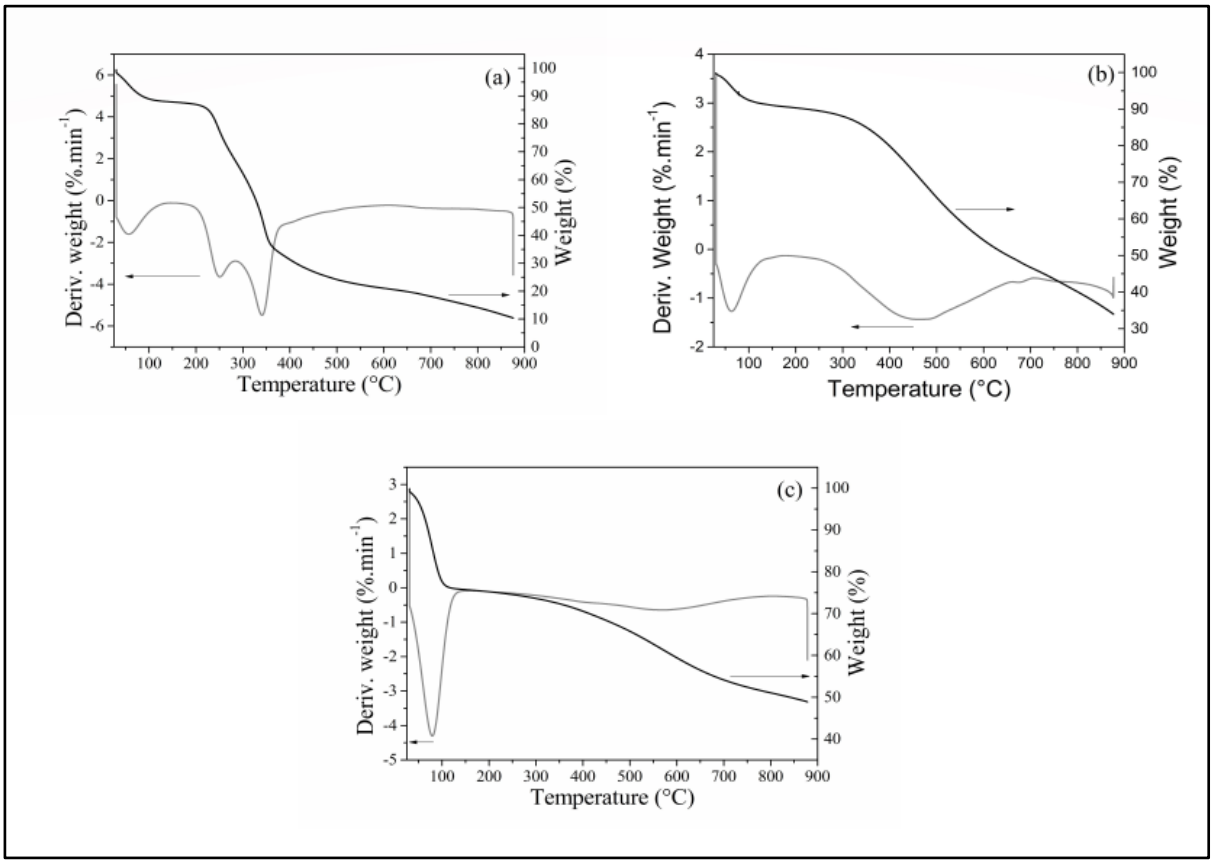

Source: Authors (2021)

According to the TG profiles, it is possible to observe three stages of mass loss. The first stage is related to water loss, the second one is pointed out to be associated with organic compounds, such as lignin, hemicellulose, and cellulose, and the third

stage is related to the decomposition of protein and fat fractions (BOLUDA-AGUILAR; LÓPEZ-GÓMEZ, 2013). Since the biosorbents C and A were exposed to the thermic treatment, the stages of mass loss are not very well defined (Fig. 2b and c, respectively) when compared to the biosorbent N.

Water represented 12% of the mass loss of the biosorbent N (120°C) (Fig. 2a). At 370°C, 53% of the mass loss was achieved and it is pointed to be related to cellulose and hemicellulose degradation. At the end of the assay, 90% of the mass was lost in the biosorbent N. The biosorbent C presented higher stability due to the thermal treatment and at the end of the assay, only 66% of mass loss was achieved in the carbonization process. Likewise, 10% of mass loss was achieved at 120°C. The decrease in mass loss rates is associated with the fact that 50% of lemon peel *in natura* is made of pectin, lignin, cellulose, and hemicellulose, which are degraded at a range of 150 to 400°C (BOLUDA-AGUILAR; LÓPEZ-GÓMEZ, 2013).

Up to 120°C, biosorbent A (Figura 3c) presented a mass loss estimated at around 25% and a total mass loss of 51% at 900°C. Mahmoodi et al. (2018) have also found three degrees in the thermal decomposition of activated kiwi peel with $ZnCl_2$ and KOH. The activated lemon peel derivative presented higher thermal stability regarding the cellulosic fraction up to 400°C due to the combined use of H_3PO_4 and temperature (250ºC) in the preparation.

The surface charge profiles of the biosorbents N, C, and A are positively charged at the surface when the pH of the medium is higher than 4.5, 7.2, and 4.0. As previously discussed, an operational pH below these values will then favor the charged surface groups and anionic molecules interactions, therefore, the adsorption of RYG over MB.

3.4 Selection of operational parameters

The biosorbent C did not present considerable removal rates of the model dyes in the synthetic samples at pH values equal to or greater than 4.

For this reason, the following assays were performed with biosorbents N and A only. The results mean that the carbonization of the biomass is not suitable for adsorption purposes. Table 1 shows the results for the removal rates at different pH conditions.

Table 1 – Removal rates of MB and RYG synthetic samples by (a) *in natura* and (b) activated lemon peel biosorbents according to the pH of the assay

	Removal rate			
pH	***In Natura***		**Activated**	
	RYG	**MB**	**RYG**	**MB**
2	56.09	100	100	100
3	14.71	100	69.07	100
4	-	100	27.99	100
5	-	100	40.63	100
6	-	100	23.47	100
7	-	100	31.60	100
8	-	100	16.25	100
9	-	100	58.69	100

Source: Authors (2021)

According to Table 1, the highest removal rates were achieved at pH = 2.0 for both N and A biosorbents. Maximum adsorption rates of MB were attained in all the preliminary assays performed. This may be explained by the cationic nature of MB molecules and their interactions with displaced π-electrons on the biosorbent surface groups as pointed out by Pereira *et al.* (2009). Aboua *et al.* (2015) have found similar results on the adsorption of methylene blue and methyl orange on macoré shells.

Vieira *et al*. (2009) evaluate textile dyes adsorption on babassu coconut mesocarp and highlighted the chemical structure of the adsorbates play a major role in adsorption capacities and selectivity. As predicted by the pH_{PZC} analysis, acidic conditions favor the adsorption of the anionic dyes which explains superior removal rates of RYG at pH = 2.0

with both lemon peel-derivatives. The mechanism of adsorption is influenced by the pore size distribution which affects the diffuse step of the operation (MAHMOODI; TAGHIZADEH; TAGHIZADEH, 2018). Thus, the removal process of RYG is more prone to be affected when compared to MB by the decrease of pore size since it presents a larger molecular structure. The effect of the charge is also to be considered.

The dosage study was analyzed by the intersection of the removal rate and adsorption capacity profiles. The results for biosorbents N and A are exhibited in Table 2.

Table 2 – Minimum and maximum biosorption capacities and removal rates regarding biosorption dosage for biosorbent N and A

Dye	**Parameters**	***In Natura***		**Activated**	
		Minimum	**Maximum**	**Minimum**	**Maximum**
MB	q ($mg.g^{-1}$)	0.32	2.06	0.59	9.86
	Removal Rate (%)	20.87	53.59	100	100
	Intersection ($g.L^{-1}$)	6		1.2	
RYG	q ($mg.g^{-1}$)	-	-	0.38	5.02
	Removal Rate (%)	-	-	80.22	100
	Intersection ($g.L^{-1}$)		-	1.6	

Source: Authors (2021)

As it can be seen by the dosage study, biosorbent N did not present efficiency in removing RYG in the model samples. These results may be related to the competition with MB. Regarding the removal rates, the biosorbent A achieved total removal of MB while the biosorbent N attained only 20.87%. At the maximum dosage, only 53.59% of removal was reached. According to biosorption capacities, biosorbent A exhibited higher affinity by MB than biosorbent N, and the effect is enhanced when the dosage is increased. For RYG, the removal rates increased to 100% by raising the dosage of activated lemon-peel carbon. The feasible dosage presented for MB was estimated at 6 $g.L^{-1}$ with N. Biosorbent A optimized dosages of 1.2 and 1.6 $g.L^{-1}$ for MB and RYG,

respectively. For this reason, the kinetic study was carried out with biosorbent A at a dosage of 1.6 $g.L^{-1}$ in order to obtain maximum results for the removal of both dyes since RYG demonstrated to limit the operation efficiency.

3.5 Kinetic modeling of model sample

The kinetic assays were performed with samples at concentrations of 5, 10, and 15 $mg.L^{-1}$ for 360 minutes at pH = 2.0 and 1. 6 $g.L^{-1}$ of biosorbent A. The kinetic profiles of each dye in each assay are displayed in Figure 3. Additionally, model fitting to PFO, PSO, and Elovich kinetic models is presented.

Figure 3 – Kinetic profiles of the MB (left) and RYG (right) biosorption in model samples at initial concentrations

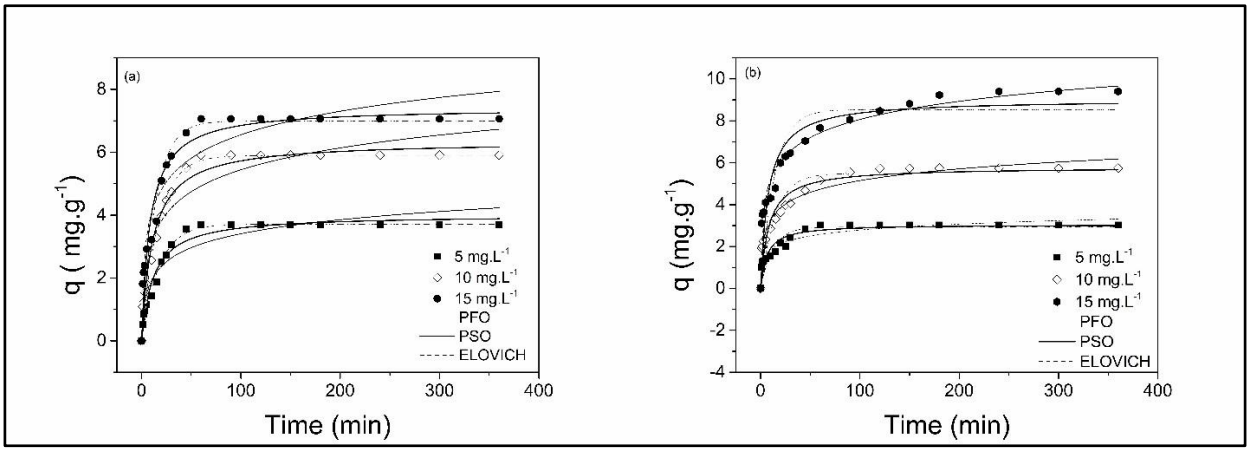

Source: Authors (2021)

The removal profiles indicated instantaneous adsorption for both dyes and the equilibrium times around 60 minutes at an initial concentration of 5 $mg.L^{-1}$. When initial concentration is increased in equimass mixtures, biosorption rates of RYG are slowed down and equilibrium is reached at 120 and 180 minutes for 10 and 15 $mg.L^{-1}$ initial concentrations, respectively. Thus, the increase in concentration favors the competitive molecule with higher affinity, which indicates the competition for common active sites on the surface of the material.

Table 3 – Kinetic fitting parameters for the biosorption of MB and RYG on activated lemon peel particles to PFO, PSO, Elovich and Intraparticle Diffusion models

Model	Parameters	RYG initial concentration ($mg.L^{-1}$)			MB initial concentration ($mg.L^{-1}$)		
		5.0	**10.0**	**15.0**	**5.0**	**10.0**	**15.0**
Experimental	q_{exp} ($mg.g^{-1}$)	2.82	5.54	9.23	3.55	5.50	6.61
PFO	q_{calc} ($mg.g^{-1}$)	2.93	5.49	8.53	3.71	5.90	6.99
	k_1 (min^{-1})	0.08	0.07	0.07	0.06	0.06	0.07
	R^2	0.83	0.84	0.79	0.98	0.98	0.93
	AICc	-32.43	-11.04	10.31	-59.04	-44.27	-16.80
PSO	q_{calc} ($mg.g^{-1}$)	3.06	5.79	9.01	4.01	6.36	7.42
	k_2 ($g.mg^{-1}.min^{-1}$)	0.05	0.02	0.01	0.02	0.01	0.02
	R^2	0.90	0.92	0.89	0.97	0.97	0.96
	AICc	-42.76	-22.81	-1.07	-50.99	-40.26	-23.00
Elovich	α ($mg.g^{-1}.min^{-1}$)	3.83	4.77	8.01	1.29	2.26	4.72
	β ($g.mg^{-1}$)	2.45	1.24	0.80	1.55	1.00	0.93
	R^2	0.94	0.97	0.98	0.92	0.93	0.93
	AICc	-49.71	-36.32	-27.06	-31.84	-17.55	-13.30
Intraparticle diffussion	k_{dif} ($mg\ g^{-1}\ min^{-1/2}$)	0.33	0.43	0.35	0.50	0.73	0.59
	C ($mg.g^{-1}$)	0.52	1.68	4.59	0.07	0.57	2.58
	R^2	0.95	0.97	0.98	0.92	0.95	0.98
	AICc	-24.43	-26.05	-28.64	-15.97	-14.59	-14.31

Source: Authors (2021)

According to Fig. 3, it is possible to observe that MB equilibrium times were reached at around 60 minutes in the three assays, which indicates the diffusion rates are not influenced by the initial concentration and the presence of the competing adsorbate in the range of concentrations in which the study was performed. PFO model demonstrated the most significant fitting for MB profiles, as well as RYG profiles at 5 and 10 $mg.L^{-1}$. However, the Elovich model demonstrated to fit better to the experimental data when the initial concentration was at 15 $mg.L^{-1}$. Table 3 exhibits the estimated parameters of each model fitting and the fitting parameters R^2 and AICc. The estimative for the Intraparticle Diffusion model is also displayed and it was calculated considering three steps in the adsorption kinetic profiles.

To evaluate the efficiency of the fitting models to the experimental data, R^2 and AICc were analyzed. According to the fitting criteria, the Elovich and intraparticle diffusion models were the best fit for RYG biosorption. Biosorption capacity for MB was expected to be greater due to its charge and molecule structure. The competition can be pointed out to cause a decline in intraparticle diffusion rates of RYG when the concentration of the competing adsorbate is enhanced (NASCIMENTO JÚNIOR; SILVA; VIEIRA, 2019). In Table 3, it can be seen for RYG biosorption that the relation $\alpha . \beta^{-1}$ is directly proportional to the initial concentration of the dye. Since α is the adsorption rate parameter and β is the desorption rate parameter, it suggests a low rate of desorption. These results corroborate the chemisorption nature of the process due to the interaction of RYG molecules and active sites.

For MB biosorption, the pseudo-first-order model demonstrated the best fitting for C_0 = 5 and 10 $mg.L^{-1}$ and considerable fitting to the 15 $mg.L^{-1}$ assay. Although the first-and second-order kinetic models were designed to describe chemical reactions, they are reported as presenting a reasonable fitting when electrons are shared or exchanged among active sites and adsorbates in complexation and ion-exchange mechanisms (MAO; IMTIAZ; ZHANG, 2015). The results indicate that the MB concentration is determining the kinetic rates and the considerable fitting to the PSO model indicates that the active site concentration also plays a role in the rate constants.

Hence, the mass transfer in the external liquid film may be the kinetic determining step at the lowest concentrations of this study and the intraparticle diffusion step may influence the process kinetics when the initial concentration of adsorbates is enhanced. Better fitting criteria for MB in the intraparticle diffusion model when C_0 is uplifted corroborates this hypothesis (NASCIMENTO JÚNIOR; SILVA; VIEIRA, 2019).

According to Taylo*r et al.* (2016), the kinetics of adsorption may be processed in three steps. The first step is characterized by high rates of mass transfer to the external film due to the higher concentration of adsorbates and the larger availability of active sites, the instantaneous adsorption. In the second step, intraparticle diffusion plays a major role in kinetic rates and the rate-limiting step is slowed down. In the last step when the equilibrium is reached, the samples are characterized by the lowest concentrations of adsorbates in the liquid phase and the intraparticle diffusion effect is negligible. The multilinear analyses of the kinetic profiles for MB and RYG are displayed in Fig. 4.

Figure 4 – Intraparticle diffusion modeling for the biosorption of RYG (a) and MB (b) for the model sample biosorption

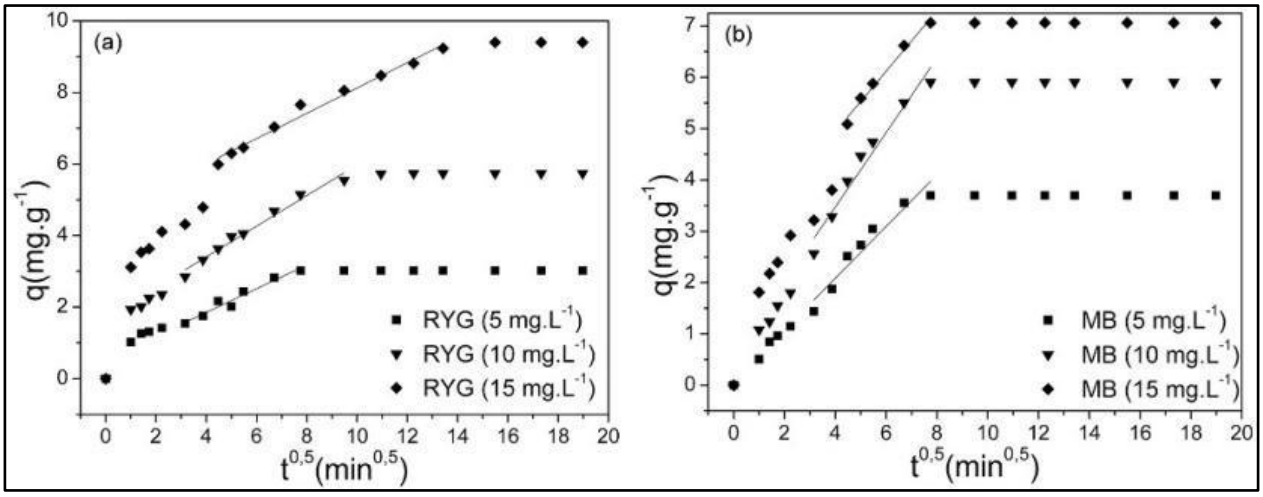

Source: Authors (2021)

Table 4 – Application of agro-industrial waste biosorbents on the removal of MB and RYG in water samples

Dye	Biosorbent	C_0 ($mg.L^{-1}$)	Dosage ($g.L^{-1}$)	Time (min)	Removal (%)	Reference
MB	Soursoup residue	50	5	300	80	Meili *et al*. 2019
	Sugarcane bagasse				90	
	Açaí biochar	20	12	120	26	Pessoa *et al*. 2019
	H_3PO_4-modified corn stalks	50	2	285	97	Tang et al. 2019
	Anionic surfactant-modified rice straw	100	0.5	120	85	Pirbazari *et al.* 2015
	Ryegrass straw	150	5	400	70	Silva *et al.* 2020
	Activated NaOH-biochar straw			150	60	
	Acid-treated banana peel	100	0.6	1440	80	Jawad *et al.* 2018
	Citrus limetta peel	250	1	180	96	Shakoor and Nasar 2018
	Sugarcane bagasse grafting maleic anhydride	400	20	120	97	Ge *et al.* 2017
	Walnut carbon	14	2.5	29	55	Hajatia *et al.* 2016
	Activated lemon peel	15	1.6	360	100	This Work
RGY	Banana peel	100	40	120	70	Nascimento *et al.* 2016
	Green coconut mesocarp				95	
	Peanut hull	100	60	120	80	Nascimento *et al.* 2014
	Orange peel				52	
	Activated lemon peel	15	1.6	360	100	This Work

Source: Authors (2021)

It can be concluded by Figure 4 that the rate-limiting step is a combination of mechanisms. The fitting for the intraparticle diffusion model allows one to estimate the thickness of the boundary layer (C) from the intersection with the Y-axis (KHALED et al., 2009). When the linear fitting of the ID model crosses the origin, intraparticle diffusion is defined to be the exclusive rate-limiting step (MAGDY, ALTAHER, 2018). The estimative of the thickness of the boundary layer increased proportionally to the initial concentration of dyes, which is expected since more adsorbate is available to interact with the solid surface of biosorbent. According to Table 3, the thickness of RYG film is magnified approximately three times while the thickness of MB is magnified five times when the initial concentration of adsorbates is increased by 5 mg.L-1 individually and 10 mg.L-1 in total. These results attest to the presence of different steps in limiting kinetic rates, a characteristic of chemically complex adsorbents.

Table 4 brings a literature review on the application of agro-industrial waste biosorbents in the removal of MB and RYG when in synthetic water samples.

The literature review was carried out with single dye systems due to the lack of binary adsorption studies for the dyes used in this study. The activated biosorbent demonstrated to be competitively efficient in the removal of synthetic dyes and it is worth mentioning the lower dosage when compared to other reports in the literature.

3.6 Textile wastewater biosorption

The operational conditions applied in the kinetic study of the model samples were repeated for the treatment of wastewater from the textile industry. The removal of molecules that absorb energy in the UV-visible spectra is demonstrated in Fig. 5.

Figure 5 – Temporal evolution of the removal of the dyes in real wastewater textile according to UV-visible spectra (pH = 2.0, dosage: 1.6 $mg.L^{-1}$)

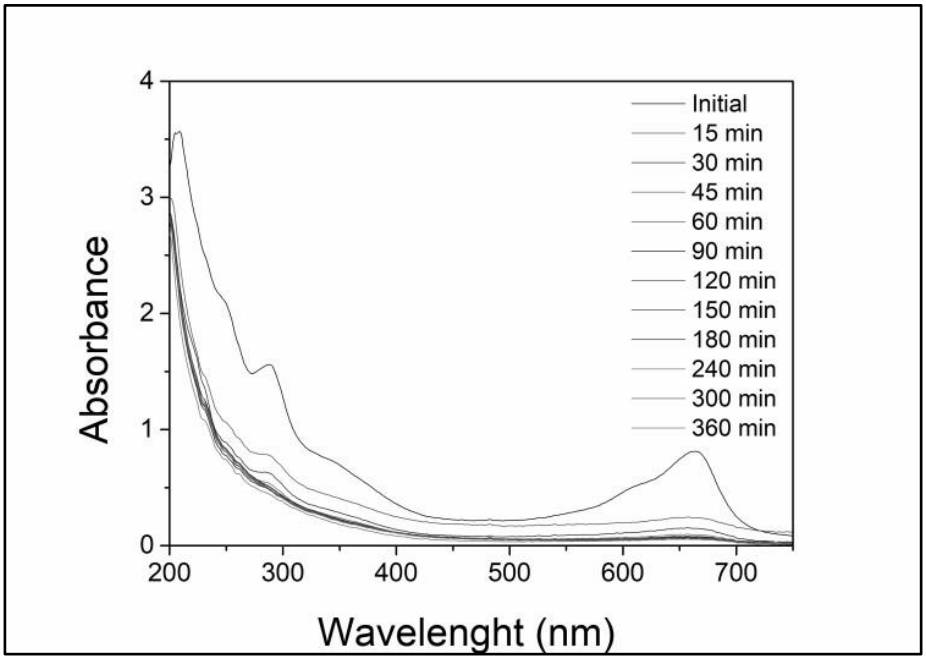

Source: Authors (2021)

According to the temporal evolution of the spectra, high removal rates of dye species were achieved after 15 minutes of operation. At 90 minutes, 88.68% of dye concentration at 664 nm was removed, and 94.22% at the end of the assay. The inferior rates of removal, when compared to the model sample, may be linked to the presence of other synthetic dyes and molecules/ions able to enhance competitivity for active sites. It is known that the textile effluent is composed of different contaminants besides synthetic dyes, such as surfactants, detergents, and other organic products (LIANG *et al*., 2017), and not all of them are removed in the primary treatment of the wastewater.

Aromatic content (the peak at 254 nm) in the wastewater was also evaluated. The presence of aromatic rings is common in synthetic dyes and they are also known by its toxicity in aqueous samples (YAGUB *et al.,* 2014). The aromatic removal presented high kinetic rates in the first 30 minutes of the assay when removal rates of 68.46% were already achieved on the activated biosorbent. At the end of the assay, 73.03% of these species were able to be removed.

3.7 Kinetic modeling of the textile wastewater biosorption

For the wastewater analysis, it could be noticed the presence of a characteristic peak around the one used to investigate the presence of MB in model samples. For this reason, the concentration of dyes was measured by the same wavelength. PFO presented the best fitting to the data among the three models, similarly to the results obtained in the synthetic samples fitting. However, the kinetic data presented only two adsorption steps. After the instantaneous adsorption step, intraparticle diffusion was attained at slower rates than the model sample biosorption. It is believed that the external mass transfer was favored since the total concentration of dyes in wastewater was estimated to be lower (7.31 $mg.L^{-1}$). Similar results were reported for the adsorption of MB on Abu-Tartour phosphate rock at lower initial concentrations, 26 and 52 $mg.L^{-1}$ (MALASH; EL-KHAIARY, 2010).

Table 5 displays the modeling parameters for further comparisons.

As it can be seen from Table 5, kinetic rates from PFO and PSO models of wastewater biosorption presented to be similar to the ones obtained in the previous kinetic study with model samples at initial concentrations of 5 e 10 mg.L-1 of each dye. The rate constant ranged from 0.01 to 0.08 min-1 (Table 3). Biosorption capacities (4.22, 4.19, and 4.48 mg.g-1) were estimated to be intermediate values among the model sample assays, which increased proportionally to initial concentration for both dyes (Table 3). According to Table 5, the most significant fitting was the PFO model with R^2 = 0.99 and AICc = -44.89.

According to the Elovich model, a considerable rise of α e β parameters can be observed in comparison to the ones in Table 3. Adsorption rates are around 12 times higher when compared to MB biosorption in the previous assays, while β is only 0.52 higher. These results indicate a preference for MB and the active site interactions in the real matrices and desorption rates are, therefore, lowered.

Table 5 – Kinetic fitting parameters for the biosorption of MB in textile wastewater on activated lemon peel particles

Model	Parameters	Wastewater
Experimental	q_{exp} (mg.g^{-1})	4.22
PFO	q_{calc} (mg.g^{-1})	4.19
	k_1 (min^{-1})	0.06
	R^2	0.99
	AICc	-44.89
PSO	q_{calc} (mg.g^{-1})	4.48
	k_2 (g.mg^{-1}.min^{-1})	0.02
	R^2	0.97
	AICc	-34.85
Elovich	α (mg.g^{-1}.min^{-1})	16.20
	β (g.mg^{-1})	2.07
	R^2	0.93
	AICc	-18.06
Intraparticle diffusion	k_{dif} (mg g^{-1} min$^{-1/2}$)	0.03
	C (mg.g^{-1})	3.74
	R^2	1
	AICc	-44.68

Source: Authors (2021)

Regarding intraparticle diffusion modeling, k_{dif} shrank when compared with Table 3 results, which indicates this step of the operation is slower in the real wastewater assay. The constant C was raised 6.5 times regarding the model samples (C_0 = 10 mg.L^{-1}), indicating the intensification of the boundary layer effects in real wastewater. Thus, external mass transfer resistance in the liquid film is playing an important role in the kinetics of real wastewater treatment.

The ANN models developed for the kinetic data are exhibited in Fig. 6.

Figure 6 – ANN model (1:2:2) to the removal of dyes in real textile wastewater with data fitting (a) and network with the parameters, weights, and bias (b)

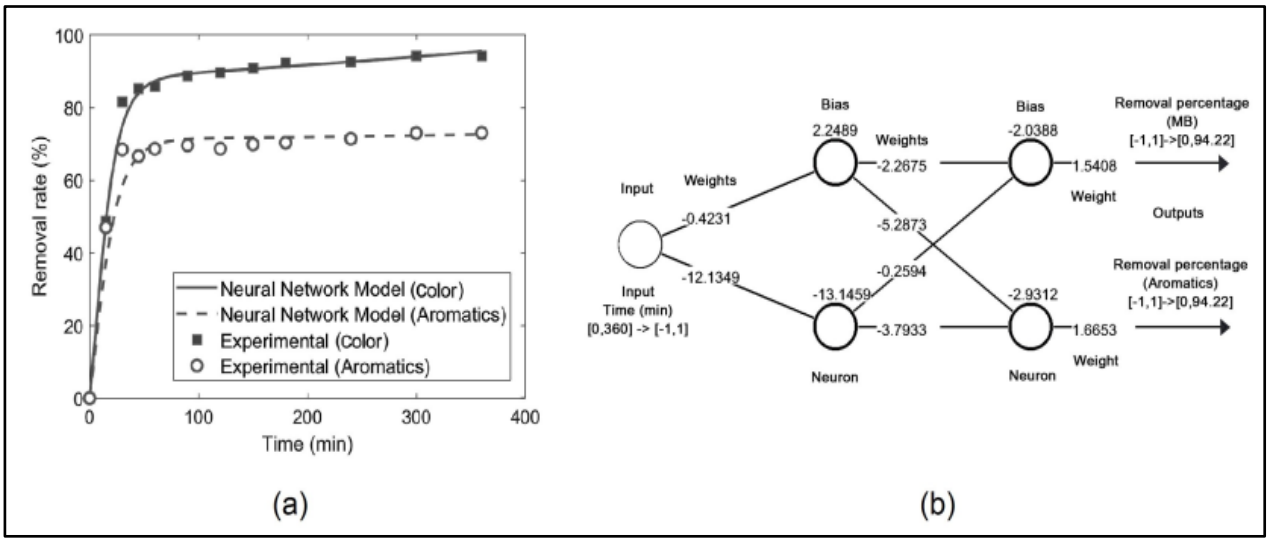

Fonte: Autores (2020)

The chart (Fig. 6a) demonstrates the correlation between the ANN models and the data. The number of hidden layers ranged from 2 to 3 neurons limited by the number of experimental data to avoid overfitting. According to the analysis of the R^2, the best fit for the data came from the network architecture described by (1:2:2) with $R^2 = 0.990$ while the (1:3:2) architecture com to $R^2 = 0.932$. The result of the adjustment for ANN was similar to that obtained for in orange peel according to AFOLABI (2020).The removal rates were decided to be set as the response (output values) so that the model after the training and validation by the software can predict the removal rates at a certain time under the same operational conditions. Fig. 6b represents the structure of the network with its parameters. Normalized input values, which represent the time of adsorption, must be multiplied by weights and added by the bias to the neuron information apply in Equation 8. The calculations are similarly processed up to the output values, which are denormalized to provide the removal rates from 0 to 100%. The pseudo-code algorithm can be seen below.

//Normalization

$$Input = \frac{\text{Output(i)}}{180} - 1$$

//Network computation

$$Output(1) = 1.540849\left(\frac{2}{1+\exp\left(-1\left(-2.267483\left(\frac{2}{1+\exp\left(-1\left(-0.4230537\cdot Input + 2.248924\right)\right)}-1\right)-5.287262\left(\frac{2}{1+\exp\left(-1\left(-12.13493\cdot Input - 13.14585\right)\right)}-1\right)-2.038793\right)\right)}-1\right)$$

$$Output(2) = 1.665268\left(\frac{2}{1+\exp\left(-1\left(-0.2593804\left(\frac{2}{1+\exp\left(-1\left(-0.4230537\cdot Input + 2.248924\right)\right)}-1\right)-3.793335\left(\frac{2}{1+\exp\left(-1\left(-12.13493\cdot Input - 13.14585\right)\right)}-1\right)-2.93124\right)\right)}-1\right)$$

//Denormalization

$$Input = \frac{\text{Output(i)}}{180} - 1$$

The training lasted three hours and required 247829 iterations. In order to upgrade the potential of the ANN model, more experiments could be carried out at different conditions of pH, dosage, and wastewater quality parameters and implemented to the model. The results are expected to allow one to predict removal rates at every operational condition in the range of assays.

4 CONCLUSIONS

It was possible to conclude that *in natura* and activated lemon peel-derivative biosorbents are feasible alternatives in the removal of the synthetic dyes in a model sample. The activation process enhanced the biosorption capacity and operational conditions could be investigated to achieve higher removal rates. Kinetic modeling of the model sample biosorption at the selected conditions revealed that different steps in the process may limit the mass transfer rates according to the dye and the initial concentration. The biosorption behavior was demonstrated to be complex and not

controlled exclusively by intraparticle diffusion. For the real textile wastewater sample, 94.22% of color was removed, corroborating with the promising application of the biosorbent in the treatment of colored wastewaters. Besides that, kinetic models could reach a desired correlation to the data. The development of ANN models proved to be a powerful tool to simulate the response of the adsorption process with high accuracy. Thus, the activated lemon peel-derivative biosorbent presented to be a feasible alternative to the minimization of agro-industrial waste and the treatment of colored wastewaters.

ACKNOWLEDGMENT

We acknowledge the financial support from CNPq and the technical support from LATECLIM/UFPE and LEA/UFPE.

REFERENCES

ABOUA, K. N.; YOBOUET, Y. A.; YAO, K. B.; GONÉ, D. L.; TROKOUREY, A. Investigation of dye adsorption onto activated carbon from the shells of Macoré fruit. J. **Environ Manage**, v. 156, p. 10–14, 2015.

AFOLABI, I. C.; POPOOLA, S. I.; BELLO, O. S. Modeling pseudo-second-order kinetics of orange peel-paracetamol adsorption process using artificial neural network. **Chemometr Intell Lab Syst**, v. 203, p. 104053, 2020.

AHMAD, A.; RAFATULLAH, M.; VAKILI, M.; MOHD-SETAPAR, S. H. Equilibrium and kinetic studies of methyl orange adsorption onto chemically treated oil palm trunk powder. **Environ Eng Manag J**, v. 17, n. 12, p. 2933–2943, 2018.

AICHOUR, A.; ZAGHOUANE-BOUDIAF, H.; IBORRA, C. V.; POLO, M. S. Bioadsorbent beads prepared from activated biomass/alginate for enhanced removal of cationic dye from water medium: Kinetics, equilibrium and thermodynamic studies. **J. Mol. Liq.**, v. 256, p. 533–540, 2018.

AMIN, N. K. Removal of direct blue-106 dye from aqueous solution using new activated carbons developed from pomegranate peel: Adsorption equilibrium and kinetics. J. **Hazard Mater**, v. 165, n. 1–3, p. 52–62, 2009.

ANDRADE, C. A.; ZAMBRANO-INTRIAGO, L. A.; OLIVEIRA, N. S.; VIEIRA, J. S.; QUIROZ-FERNÁNDEZ, L. S.; RODRÍGUEZ-DÍAZ, J. M. Adsorption Behavior and Mechanism of Oxytetracycline on Rice Husk Ash: Kinetics, Equilibrium, and Thermodynamics of the Process. **Water Air Soil Pollut**, v. 231, n. 3, 2020.

AQUINO, R. V. S.; BARBOSA, A. A.; RIBEIRO, L. B.; OLIVEIRA, A. F. B.; SILVA, J. P.; AZOUBEL, P. M.; ROCHA, O. R. S. Degradation of leaf green food dye by heterogeneous photocatalysis with TiO2 over a polyethylene terephthalate plate. **Chem Pap**, v. 73, n. 10, p. 2501–2512, 2019.

BARBOSA, A. A.; AQUINO, R. V. S. DE; FLÁVIA, A.; OLIVEIRA, B.; DANTAS, R. F.; SILVA, J. P.; DUARTE, M. M. M. B.; OTIDENE, R. S. Development of a new photocatalytic reactor built from recyclable material for the treatment of textile industry effluents. **Desalin Water Treat**,v. 151, p. 82-92, 2019.

BAUTISTA-TOLEDO, M. I.; RIVERA-UTRILLA, J.; MÉNDEZ-DÍAZ, J. D.; SÁNCHEZ-POLO, M.; CARRASCO-MARÍN, F. Removal of the surfactant sodium dodecylbenzenesulfonate from water by processes based on adsorption/bioadsorption and biodegradation. J. **Colloid Interface Sci.**, v. 418, p. 113–119, 2014.

BELLO, O. S.; AHMAD, M. A.; SEMIRE, B. Scavenging malachite green dye from aqueous solutions using pomelo (Citrus grandis) peels: kinetic, equilibrium and thermodynamic studies. **Desalin Water Treat**, v. 56, n. 2, p. 521–535, 2015.

BERGSTRA, J.; BENGIO, Y. Random search for hyper-parameter optimization. **J Mach Learn Res**, v. 13, p. 281–305, 2012.

BHATNAGAR, A.; KUMAR, E.; MINOCHA, A. K.; JEON, B. H.; SONG, H.; SEO, Y. C. Removal of anionic dyes from water using citrus limonum (lemon) peel: Equilibrium studies and kinetic modeling. **Sep Sci Technol**, v. 44, n. 2, p. 316–334, 2009.

BISHOP, C.M. **Neural networks for pattern recognition**, Claredon Press, Oxford, 1996.

BOLUDA-AGUILAR, M.; LÓPEZ-GÓMEZ, A. Production of bioethanol by fermentation of lemon (Citrus limon L.) peel wastes pretreated with steam explosion. **Ind Crops Prod**, v. 41, n. 1, p. 188–197, 2013.

BONATE, P.L Pharmacokinetic and Pharmacodynamic Modeling and Simulation. 2 ed. E New York, Springer, 2011

BRITO, M. J. P.; VELOSO, C. M.; SANTOS, L. S.; BONOMO, R. C. F.; FONTAN, R. DA C. I. Adsorption of the textile dye Dianix® royal blue CC onto carbons obtained from yellow mombin fruit stones and activated with KOH and H3PO4: kinetics, adsorption equilibrium and thermodynamic studies. **Powder Technol.**, v. 339, p. 334–343, 2018.

CHIENG, H. I.; LIM, L. B. L.; PRIYANTHA, N. Enhancing adsorption capacity of toxic malachite green dye through chemically modified breadnut peel: Equilibrium, thermodynamics, kinetics and regeneration studies. **Environ Technol**, v. 36, n. 1, p. 86–97, 2015.

DEHGHANI, M. H.; SANAEI, D.; ALI, I.; BHATNAGAR, A. Removal of chromium(VI) from aqueous solution using treated waste newspaper as a low-cost adsorbent: Kinetic modeling and isotherm studies. **J. Mol. Liq.**, v. 215, p. 671–679, 2016.

DENG, H.; ZHANG, G.; XU, X.; TAO, G.; DAI, J. Optimization of preparation of activated carbon from cotton stalk by microwave assisted phosphoric acid-chemical activation. **J. Hazard. Mater.**, v. 182, n. 1–3, p. 217–224, 2010.

GE, M.; DU, M.; ZHENG, L.; WANG, B.; ZHOU, X.; JIA, Z.; HU, G.; JAHANGIR ALAM, S. M. A maleic anhydride grafted sugarcane bagasse adsorbent and its performance on the removal of methylene blue from related wastewater. **Mater. Chem. Phys.**, v. 192, p. 147–155, 2017.

GHIBATE, R.; SENHAJI, O.; TAOUIL, R. Kinetic and thermodynamic approaches on Rhodamine B adsorption onto pomegranate peel. Case Studies in **Chemical and Environmental Engineering**, v. 3, n. November 2020, p. 100078, 2021.

GISI, S. DE; LOFRANO, G.; GRASSI, M.; NOTARNICOLA, M. Characteristics and adsorption capacities of low-cost sorbents for wastewater treatment: A review. **Sustain Mater Techno**, v. 9, p. 10–40, 2016.

GOSWAMI, M.; PHUKAN, P. Enhanced adsorption of cationic dyes using sulfonic acid modified activated carbon. J. Environ**. Chem**. **Eng.**, v. 5, n. 4, p. 3508–3517, 2017.

HAJATIA, S.; GHAEDIB, M.; MAZAHERIB, H. Removal of methylene blue from aqueous solution by walnut carbon: optimization using response surface methodology. Desalin. **Water Treat**, v. 57, p. 3179-2193, 2016.

HISAINDEE, S.; MEETANI, M. A.; RAUF, M. A. Application of LC-MS to the analysis of advanced oxidation process (AOP) degradation of dye products and reaction mechanisms. Trac - **Trend Anal Chem**, v. 49, p. 31–44, 2013.

HOLKAR, C. R.; JADHAV, A. J.; PINJARI, D. V.; MAHAMUNI, N. M.; PANDIT, A. B. A critical review on textile wastewater treatments: Possible approaches. **J. Environ. Manag.**, v. 182, p. 351–366, 2016.

JAWAD, A. H.; RASHID, R. A.; ISHAK, M. A. M.; ISMAIL, K. Adsorptive removal of methylene blue by chemically treated cellulosic waste banana (Musa sapientum) peels . J. Taibah Univ. **Sci.**, v. 12, n. 6, p. 809–819, 2018.

KHALED, A.; NEMR, A. EL; EL-SIKAILY, A.; ABDELWAHAB, O. Removal of Direct N Blue-106 from artificial textile dye effluent using activated carbon from orange peel: Adsorption isotherm and kinetic studies. **J. Hazard. Mater.**, v. 165, n. 1–3, p. 100–110, 2009.

LI, Z.; WANG, G.; ZHAI, K.; HE, C.; LI, Q.; GUO, P. Methylene blue adsorption from aqueous solution by loofah sponge-based porous carbons. **Colloids Surf A**, v. 538, n. October 2017, p. 28–35, 2018.

LIANG, J.; NING, X. AN; KONG, M.; LIU, D.; WANG, G.; CAI, H.; SUN, J.; ZHANG, Y.; LU, X.; YUAN, Y. Elimination and ecotoxicity evaluation of phthalic acid esters from textile-dyeing wastewater. **Environ. Pollut.**, v. 231, p. 115–122, 2017.

LOW, S. K.; TAN, M. C. Dye adsorption characteristic of ultrasound pre-treated pomelo peel. J. Environ. **Chem. Eng.**, v. 6, n. 2, p. 3502–3509, 2018.

LUTPI, N. A.; JAMIL, N. N.; ABDULLAH, C. K. K. C. K.; WONG, Y. S.; ONG, S. A.; IZHAR, T. N. T. Sorption of Methylene Blue and Acid Orange 7 onto Ananas Peels and Leaves Based Activated Carbon. **Appl. Mech. Mater.**, v. 330, p. 112–116, 2013.

MAGDY, Y. H.; ALTAHER, H. Kinetic analysis of the adsorption of dyes from high strength wastewater on cement kiln dust. J. Environ. **Chem. Eng.**, v. 6, n. 1, p. 834–841, 2018.

MAHMOODI, N. M.; TAGHIZADEH, M.; TAGHIZADEH, A. Mesoporous activated carbons of low-cost agricultural bio-wastes with high adsorption capacity: Preparation and artificial neural network modeling of dye removal from single and multicomponent (binary and ternary) systems. **J. Mol. Liq.**, v. 269, p. 217–228, 2018.

MALASH, G. F.; EL-KHAIARY, M. I. Methylene blue adsorption by the waste of Abu-Tartour phosphate rock. J. Colloid Interface **Sci.**, v. 348, n. 2, p. 537–545, 2010.

MAO, C.; IMTIAZ, S. A.; ZHANG, Y. Competitive adsorption of Ag (I) and Cu (II) by tripolyphosphate crosslinked chitosan beads. J. Appl. Polym. **Sci.**, v. 132, n. 43, p. 1–11, 2015.

MEILI, L.; LINS, P. V. S.; COSTA, M. T.; ALMEIDA, R. L.; ABUD, A. K. S.; SOLETTI, J. I.; DOTTO, G. L.; TANABE, E. H.; SELLAOUI, L.; CARVALHO, S. H. V.; ERTO, A. Adsorption of methylene blue on agroindustrial wastes: Experimental investigation and phenomenological modelling. Prog. Biophys. **Mol. Biol.**, v. 141, p. 60–71, 2019.

NASCIMENTO, G. E. DO; CAMPOS, N. F.; SILVA, J. J. DA; BARBOSA, C. M. B. DE M.; DUARTE, M. M. M. B. Adsorption of anionic dyes from an aqueous solution by banana peel and green coconut mesocarp. **Desalin Water Treat**, v. 57, n. 30, p. 14093–14108, 2016.

NASCIMENTO, G. E. DO; DUARTE, M. M. M. B.; CAMPOS, N. F.; ROCHA, O. R. S. DA; SILVA, V. L. DA. Adsorption of azo dyes using peanut hull and orange peel: A comparative study. **Environ. Technol.**, v. 35, n. 11, p. 1436–1453, 2014.

NASCIMENTO-JÚNIOR, W. J.; SILVA, M. G. C.; VIEIRA, M. Environmental Science and Pollution Research Competitive biosorption of Cu2 + and Ag + ions on brown macro-algae waste : Kinetic and ion-exchange studies. Environ. **Sci.** Pollut. Res., 2019.

NAYAK, S. S.; MIRGANE, N. A.; SHIVANKAR, V. S.; PATHADE, K. B.; WADHAWA, G. C. Adsorption of methylene blue dye over activated charcoal from the fruit peel of plant hydnocarpus pentandra. Materials Today: **Proceedings**, v. 37, n. Part 2, p. 2302–2305, 2020.

PEREIRA, A. P. DOS S.; SILVA, M. H. P. DA; LIMA JÚNIOR, É. P.; PAULA, A. DOS S.; TOMMASINI, F. J. Processing and Characterization of PET Composites Reinforced With Geopolymer Concrete Waste. Mat. **Res.**, v. 20, n. suppl 2, p. 411–420, 2017.

PEREIRA, M. F. R.; SOARES, S. F.; ÓRFÃO, J. J. M.; FIGUEIREDO, J. L. Adsorption of dyes on activated carbons: Influence of surface chemical groups. **Carbon**, v. 41, n. 4, p. 811–821, 2003.

PESSÔA, T. S.; LIMA FERREIRA, L. E. DE; SILVA, M. P. DA; PEREIRA NETO, L. M.; NASCIMENTO, B. F. DO; FRAGA, T. J. M.; JAGUARIBE, E. F.; CAVALCANTI, J. V.; MOTTA SOBRINHO, M. A. DA. Açaí waste beneficing by gasification process and its employment in the treatment of synthetic and raw textile wastewater. **J. Clean. Prod.**, v. 240, 2019.

PIRBAZARI, P. M.; KISOMI, B. F. Co/TiO2 nanoparticles: preparation, characterization and its application for photocatalytic degradation of methylene blue. **Desalin Water Treat**, v. 63. p. 283–292, 2017.

SAEED, A.; SHARIF, M.; IQBAL, M. Application potential of grapefruit peel as dye sorbent: Kinetics, equilibrium and mechanism of crystal violet adsorption. **J. Hazard. Mater.**, v. 179, n. 1–3, p. 564–572, 2010.

SAHIBZADA, K. I.; SAEED, A.; KALIM, I.; IQBAL, M. Ion-exchange mechanism in biosorption of Pb2+ ions from contaminated water by banana stalk waste. **Environ Eng Manag J**, v. 15, n. 12, p. 2741–2751, 2016.

SANDOVAL, A.; HERNÁNDEZ-VENTURA, C.; KLIMOVA, T. E. Titanate nanotubes for removal of methylene blue dye by combined adsorption and photocatalysis. **Fuel**, v. 198, p. 22–30, 2017.

SHAKOOR, S.; NASAR, A. Adsorptive decontamination of synthetic wastewater containing crystal violet dye by employing Terminalia arjuna sawdust waste. **Groundw. Sustain. Dev.**, v. 7, n. March, p. 30–38, 2018.

SHARMA, A.; SYED, Z.; BRIGHU, U.; GUPTA, A. B.; RAM, C. Adsorption of textile wastewater on alkali-activated sand. **J. Clean. Prod**, v. 220, p. 23–32, 2019.

SHARMA, K.; VYAS, R. K.; SINGH, K.; DALAI, A. K. Degradation of a synthetic binary dye mixture using reactive adsorption: Experimental and modeling studies. J. Environ. **Chem. Eng.**, v. 6, n. 5, p. 5732–5743, 2018.

SILVA, E. O. DA; SANTOS, V. D. DOS; ARAUJO, E. B. DE; GUTERRES, F. P.; ZOTTIS, R.; FLORES, W. H.; ALMEIDA, A. R. F. DE. Removal of methylene blue from aqueous solution by ryegrass straw. Int J Environ **Sci Technol**, v. 17, n. 8, p. 3723–3740, 2020.

SOLOMONS, T.W.G., FRYHLE, C.B. **Organic Chemistry**, 10. ed., New York, John Wiley & Sons, 2012.

SUDAMALLA, P.; PICHIAH, S.; MANICKAM, M. Responses of surface modeling and optimization of Brilliant Green adsorption by adsorbent prepared from Citrus limetta peel. **Desalin Water Treat**, v. 50, n. 1–3, p. 367–375, 2012.

TANG, Y.; ZHAO, Y.; LIN, T.; LI, Y.; ZHOU, R.; PENG, Y. Adsorption performance and mechanism of methylene blue by H3PO4- modified corn stalks. J. Environ. **Chem. Eng.**, v. 7, n. 6, p. 103398, 2019.

TAYLOR, P.; RAMANA, D. K. V.; MIN, K**. Desalination and Water Treatment Activated carbon produced from pigeon peas hulls waste as a low-cost agro-waste adsorbent for Cu (II) and Cd (II) removal.** n. May, p. 37–41, 2015.

THOMMES, M.; KANEKO, K.; NEIMARK, A. V.; OLIVIER, J. P.; RODRIGUEZ-REINOSO, F.; ROUQUEROL, J.; SING, K. S. W. Physisorption of gases, with special reference to the evaluation of surface area and pore size distribution (IUPAC Technical Report). Pure Appl. **Chem.**, v. 87, n. 9–10, p. 1051–1069, 2015.

VIEIRA, A.P., SANTANA, S. A. A., BEZERRA, C. W. B., SILVA, H. A. S., CHAVES, J. A. P., MELO, J. C. P. DE, EDSON, C., FILHO, S., AND AIROLDI, C. **Kinetics and thermodynamics of textile dye adsorption from aqueous solutions using babassu coconut mesocarp.** v. 166, p. 1272–1278, 2009.

WANG, X.; JIANG, C.; HOU, B.; WANG, Y.; HAO, C.; WU, J. Carbon composite lignin-based adsorbents for the adsorption of dyes. **Chemosphere**, v. 206, p. 587–596, 2018.

WEBER, W.J.; MORRIS, J.C. Kinetics of adsorption on carbon from solutions. **J Sanit Eng Div**, v. 89, p. 31-60, 1963.

YAGUB, M. T.; SEN, T. K.; AFROZE, S.; ANG, H. M. Dye and its removal from aqueous solution by adsorption: A review. Adv. Colloid Interface **Sci.**, v. 209, p. 172–184, 2014.

ZHANG, J.; GAO, J.; CHEN, Y.; HAO, X.; JIN, X. **Characterization, preparation, and reaction mechanism of hemp stem based activated carbon.** Results Phys., v. 7, p. 1628–1633, 2017.

Authorship contributions

1 – Naiana Santos da Cruz Santana Neves

Engenheira Química pela UFPE (2016). Mestre em Engenharia Química pela UFPE (2019). Atualmente, é doutoranda pelo Programa de Pós-Graduação em Engenharia Química da UFPE.
https://orcid.org/0000-0001-8494-8058 • naiana.santana@hotmail.com
Contribuition: Writing – original draft | Methodology | Research

2 – Ramon Vinícius Santos De Aquino
Químico Industrial pela UFPE (2018). Mestre em Engenharia Química pela UFPE (2021).
https://orcid.org/0000-0003-4784-3251 • viniciusramon59@gmail.com
Contribuition: Writing – review & editing

3 – Ingrid Larissa Silva Santana
Engenheira Química pela UFPE (2019). Mestre em Engenharia Química pela UFPE (2022). Atualmente, é doutoranda pelo Programa de Pós-Graduação em Engenharia Química da UFPE
https://orcid.org/0000-0001-8545-6637 • santanasingrid@gmail.com
Contribuition: Writing | Methodology | review & editing

4 – Welenilton José Do Nascimento Júnior
Químico Industrial pela UFPE (2017). Mestre em Engenharia Química pela Unicamp (2019). Atualmente, é Professor Assistente no Departamento de Química Fundamental (UFPE) e doutorando pelo Programa de Pós-Graduação em Engenharia Química da UFPE.
https://orcid.org/0000-0003-4403-6702 • welenilton@gmail.com
Contribuition: Writing – review & editing

5 – Ada Azevedo Barbosa
Engenheira de Alimentos pela UESB (2011). Mestre em Engenharia de Alimentos pela UESB (2013). Engenheira Química pela UNINASSAU (2019). Doutora em Engenharia Química pela UFPE (2019).
https://orcid.org/0000-0002-9169-0574 • adabarbosa@hotmail.com
Contribuition: Supervision

6 – Rafaela Ferreira Carvalho
Atualmente, graduanda em Químico Industrial pela UFPE.
https://orcid.org/0000-0003-2794-9614 • rafaelaferreiradecarvalho@gmail.com
Contribuition: Writing | Methodology | review & editing

7 – Josivan Pedro Silva
Engenheiro Químico pela UFPE (2010). Mestre em Engenharia Química pela UFPE (2013). Doutor em Engenharia Química pela UFPE (2018).
https://orcid.org/0000-0003-3294-9352 • josivan_silva@hotmail.com
Contribuition: review & editing

8 – Mohand Benachour
Engenheiro Químico pela Ecole Nationale Polytechnique D Alger (1984). Mestre pela Universitè de Technologie de Compiègne (1985). Doutor em Génie Des Procédés pelo Institut National Polytéchnique de Lorraine (1990). Atualmente é professor titular da Universidade Federal de Pernambuco.
https://orcid.org/0000-0003-0139-9888 • mohand.benachour@ufpe.br
Contribuition: Supervision | Writing – review & editing

9 – Otidene Rossiter Sá Da Rocha
Engenheira Química pela UFPE (2004), Mestre em Engenharia Química pela UFRN (2007) e Doutora em Engenharia Química pela UFRN (2010). Atualmente é professor adjunto do Departamento de Engenharia Química da UFPE.
https://orcid.org/0000-0001-5216-1752 • otidene@hotmail.com
Contribuition: Supervision

How to quote this article

NEVES, N. S. da C. S.; AQUINO, R. V. S. de; SANTANA, I. L. S.; JÚNIOR, W. J. do N.; BARBOSA, A. A.; CARVALHO, R. F.; SILVA, J. P.; BENACHOUR, M.; OTIDENE, R. S. da R. Biosorption textile wastewater employing lemon peel derivatives: data analysis and kinetic modeling. **Ciência e natura**, Santa Maria, v. 26, e2, 2022. Available from: https://doi.org/10.5902/2236117065265.